英文原版

Haber ▪ Gattuso ▪ Spitz ▪ David

外科病理鉴别诊断

DIFFERENTIAL DIAGNOSIS IN SURGICAL PATHOLOGY

人民卫生出版社

Health Science Asia, Elsevier Science

Meryl H. Haber, M.D.
Borland Professor and
Chairman of Pathology
(retired)
Rush-Presbyterian-St. Luke's
Medical Center
Chicago, Illinois

Paolo Gattuso, M.D.
Associate Professor of
Pathology
Director of Anatomic
Pathology
Rush Medical College
Rush-Presbyterian-St. Luke's
Medical Center
Chicago, Illinois

Daniel J. Spitz, M.D.
Hillsborough County
Medical Examiner
Department
University of South Florida
Department of Pathology
Tampa, Florida

Odile David, M.D.
Tulane University School of
Medicine
Department of Pathology
New Orleans, Louisiana

DIFFERENTIAL DIAGNOSIS IN SURGICAL PATHOLOGY

人民卫生出版社
Health Science Asia, Elsevier Science

人民卫生出版社
Health Science Asia, Elsevier Science

DIFFERENTIAL DIAGNOSIS IN SURGICAL PATHOLOGY
Original English Language Edition

图书在版编目(CIP)数据

外科病理鉴别诊断/(美)哈博编著.—修订本.—北京：人民卫生出版社，2002
ISBN 7-117-04922-7

Ⅰ.外… Ⅱ.哈… Ⅲ.外科学：病理学-鉴别诊断-英文 Ⅳ.R602

中国版本图书馆 CIP 数据核字(2002)第 024021 号

图字：01-2002-1965

外科病理鉴别诊断(英文版)

编　　著：Meryl H. Haber, M. D. 等
出版发行：人民卫生出版社(中继线 67616688)
地　　址：(100078)北京市丰台区方庄芳群园 3 区 3 号楼
网　　址：http://www.pmph.com
E-mail：pmph@pmph.com
印　　刷：北京市安泰印刷厂
经　　销：新华书店
开　　本：889×1194　1/16　**印张**：71　**插页**：8
字　　数：3364 千字
版　　次：2002 年 8 月第 1 版　2002 年 8 月第 1 版第 1 次印刷
标准书号：ISBN7-117-04922-7/R·4923
定　　价：234.00 元

Preface

Nearly three years ago a small contingent of senior residents and an attending pathologist approached me as Chairman of the Department of Pathology at Rush with the idea of writing a new and different type of textbook on diagnostic surgical pathology. They wanted my support and assistance. Hoping to encourage them, and not wanting to discourage them, I needed to know more about their ideas for something "new and different" and why, in a field already populated with several excellent textbooks on the subject, a new textbook would be a worthwhile addition to the surgical pathologist's library. At this first meeting I felt it was my duty to inform them of the many difficulties in embarking on such a venture, not the least of which would be the excessive amount of time and effort required and the fact that, in the end, a publisher might not be willing to take the final product to market. They persisted in their arguments about how valuable and worthwhile a book this would eventually become and outlined their concepts for the final product. By the end of this first meeting, and more convincingly after several others, I believed that this group of residents and staff had formulated the ideas for a new textbook that would, upon completion, be a significant resource for pathologists, those in training and in practice, and others interested in surgical pathology. After reviewing and approving a prototypical chapter, I felt certain that this text would be worthy of the efforts of these individuals. I gave my go-ahead, along with a promise that I would assist in the writing, editing and helping to see this work through to the end.

The authors believe that the readers of this textbook will find it helpful in teaching how to approach and deal with diagnostic problems in surgical pathology and will assist a more experienced examiner in arriving at an expedient, correct, and accurate diagnosis. Many useful and unique features are included as aids to diagnoses. A traditional organization by organ system is employed. Each chapter begins with an algorithm tracing a differential diagnostic approach a pathologist might follow in reviewing a surgical specimen in order to arrive at an accurate diagnosis. The algorithm directs the reader to the many and varied options that might be considered in this process. The resident pathologist, fellow or junior attending will find these algorithms most useful since it is the inexperienced individual who may, for example, have difficulty in deciding whether a lesion is inflammatory or neoplastic, and if one or the other, exactly what specific pathologic diagnosis is most appropriate. The algorithms are also helpful for the experienced pathologist who might more aptly appreciate the nuances in arriving at a correct diagnosis.

This book is not intended to serve as a comprehensive encyclopedia of all possible pathologic entities in every organ system. However, many of the more frequently observed surgical pathologic conditions are described in an outline formatted text and illustrated with nearly 1000 gross and microscopic photographs, both black and white and color. The illustrations are appropriately interspersed along side each of the diagnostic entities discussed. Each photograph was selected and reproduced with great care in order to provide the necessary diagnostic information to enable the observer to accurately identify a specific entity and to differentiate it from other, sometimes confusing, similar

conditions. The authors have found that this format—algorithm:descriptive text: illustration—is most helpful in the identification and diagnosis of the many difficult differential diagnostic problems encountered in the operating room by the surgeon or in the pathology laboratory by the pathologist. We hope that the readers of this textbook will feel similarly.

Meryl H. Haber, M.D.

Acknowledgments

This textbook is the work of many, but none have worked as hard to achieve its completion as Paolo Gattuso, M.D. In addition to his many duties in an academic Department of Pathology in a busy medical center, Dr. Gattuso has spent many untold hours in authoring, editing, composing, and proofreading the manuscript. His unstinting devotion to the task of getting the various authors to complete their sections and chapters, as well as refining and selecting many of the most appropriate illustrations, must be acknowledged. Additionally, mention must also be made of the exceptional efforts of Daniel J. Spitz, M.D., who, initially as a pathology resident, then a fellow, and most recently a forensic pathologist found the time and energy to contribute extensively to the text and to formulate many of the algorithms which are included with each chapter.

The authors wholeheartedly thank Christine Spano and Lupe Alcala who spent many hours typing and organizing the manuscript. Dorothy Forbes, Josef Heller, M.D., and Diana Treaba, M.D. assisted in the development and completion of this project, and we owe them much thanks. We are also indebted to our editor at Saunders, Marc Strauss, for his unstinting cooperation and encouragement throughout the production of this textbook.

Meryl H. Haber, M.D.

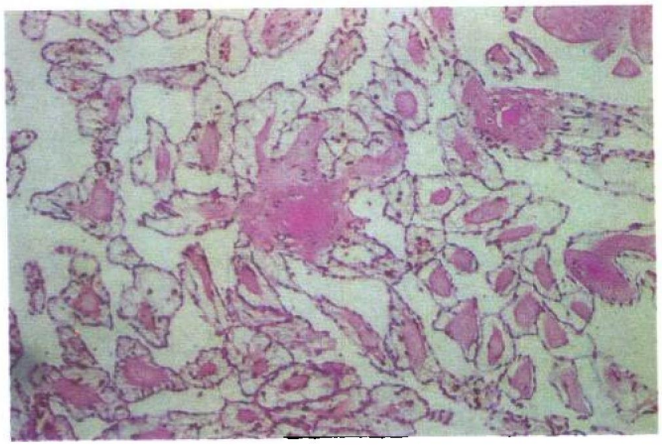

Color Plate 1. **Papillary fibroelastoma.** Histologic section shows branching outgrowths with avascular fibroelastic cores. (See page 22, Fig. 1–9.)

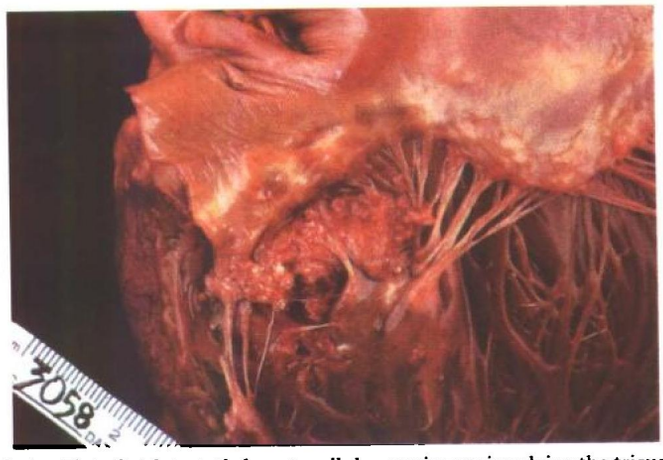

Color Plate 2. Metastatic hepatocellular carcinoma involving the tricuspid valve. (See page 28, Fig. 1–16.)

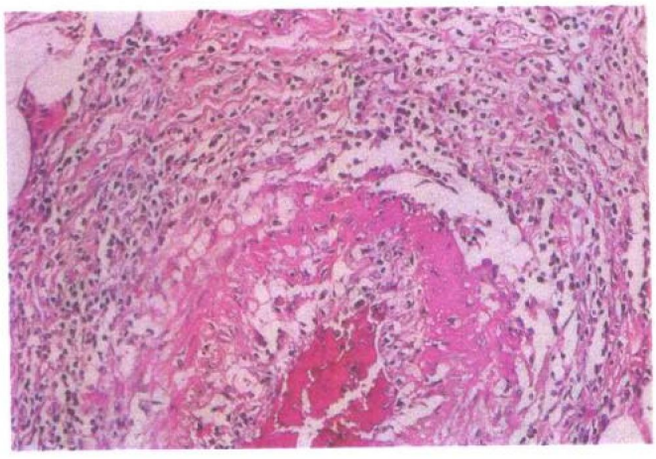

Color Plate 3. **Polyarteritis nodosa.** Histologic section of medium-sized blood vessel shows transmural infiltrate of acute and chronic inflammatory cells and fibrinoid necrosis. (See page 31, Fig. 1–18.)

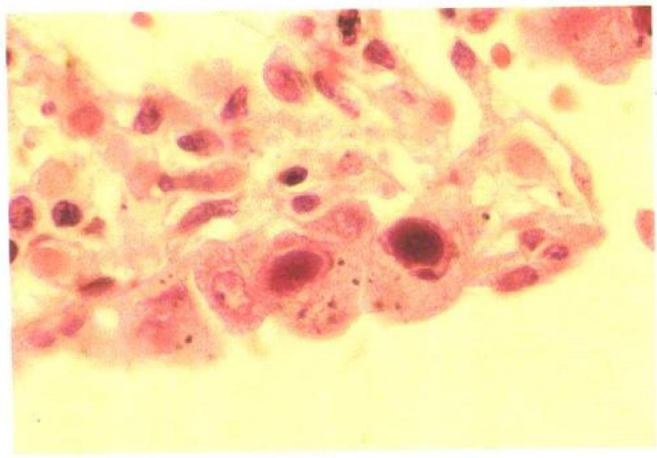

Color Plate 4. **CMV pneumonia.** In the center of the picture there are two enlarged cells, each with a single large intranuclear inclusion, perinuclear halo or clearing, and multiple small intracytoplasmic inclusions, which are diagnostic for CMV. (See page 55, Fig. 2–10A.)

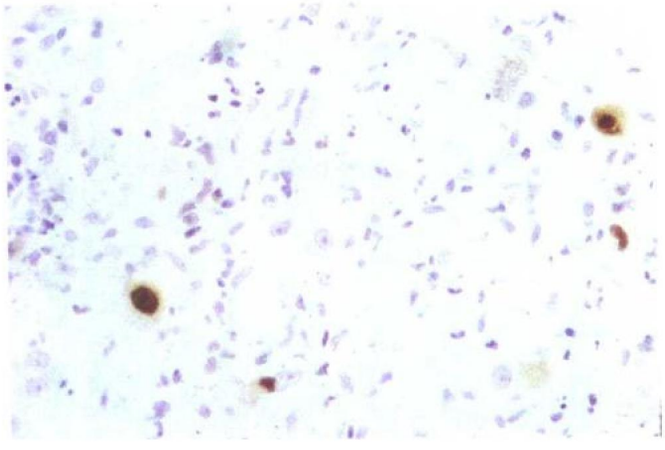

Color Plate 5. **CMV pneumonia.** Immunoperoxidase stain using antibody mixture against immediate-early and early nuclear antigens stains not only the enlarged nuclei but also infected normal-sized nuclei that are not yet showing the cytopathic effect of CMV. This allows for early diagnosis of CMV when diagnostic inclusions are not present in the biopsy. (See page 55, Fig. 2–10B.)

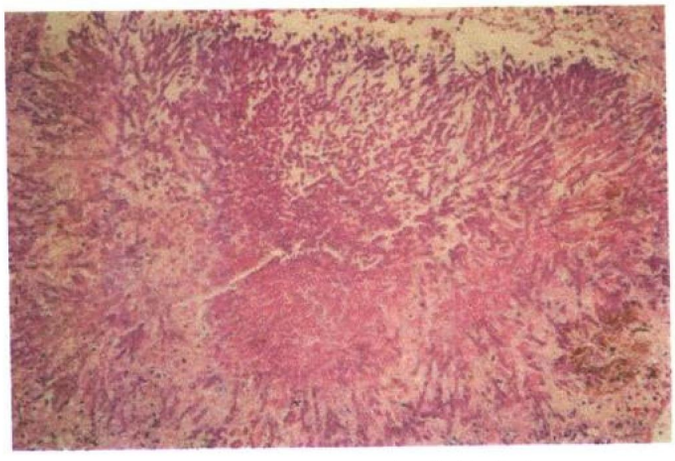

Color Plate 6. **Fungal infection: aspergillosis.** Radiating arrangement of fungal hyphae with central necrosis can be easily seen on H&E stain. (See page 57, Fig. 2–12A.)

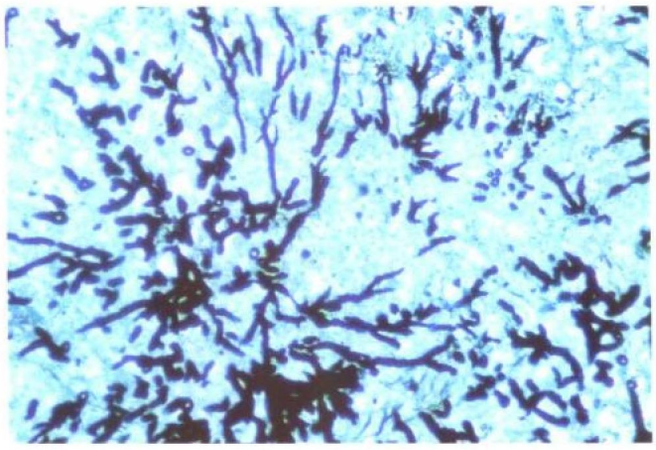

Color Plate 7. **Fungal infection: aspergillosis.** GMS stain shows characteristic hyphae with parallel walls and acute angle branching. (See page 57, Fig. 2–12B.)

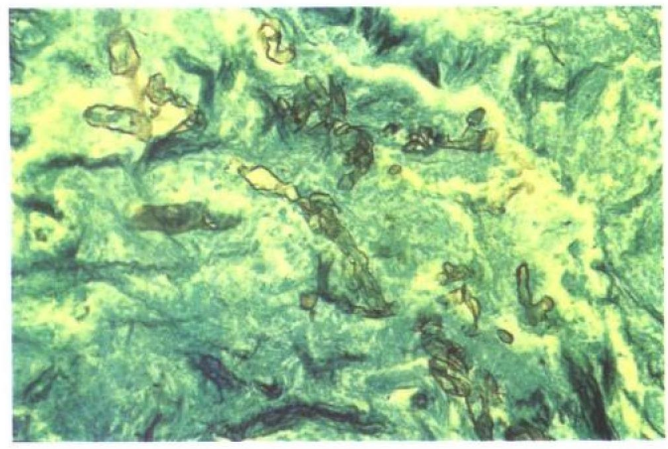

Color Plate 8. **Fungal infection: mucormycosis.** GMS stain shows broad wavy ribbon-like hyphae, some with 90° branching. (See page 58, Fig. 2–13.)

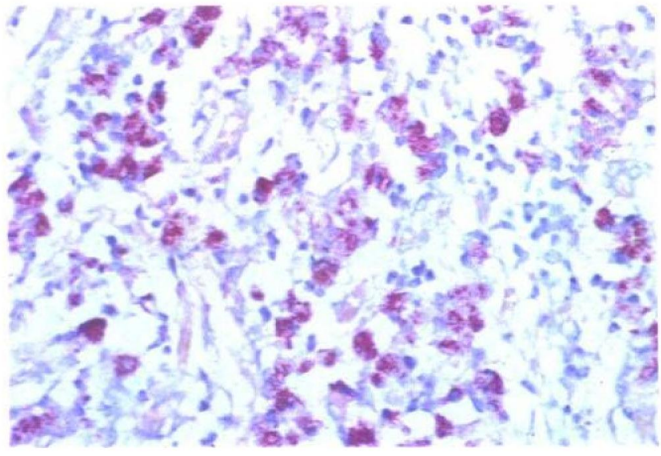

Color Plate 9. **Atypical mycobacterial pneumonia.** Acid-fast stain demonstrates numerous bright pink intracellular organisms, which can be easily seen at low power in this biopsy specimen from an AIDS patient. (See page 59, Fig. 2–15.)

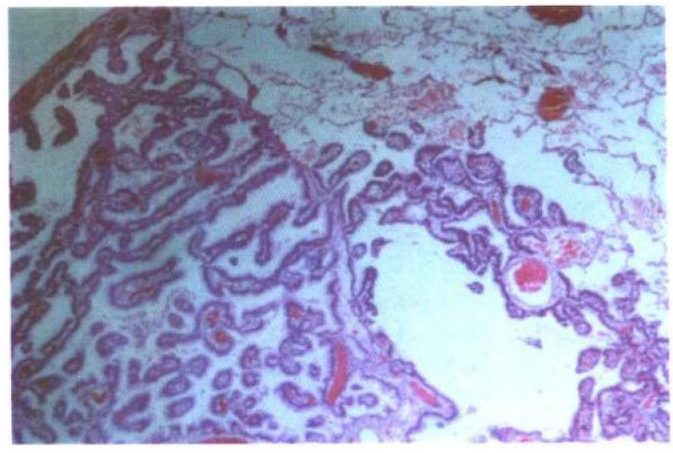

Color Plate 10. **Bronchioloalveolar carcinoma.** Tumor cells are lining pre-existing septa with no desmoplastic reaction (low power). (See page 98, Fig. 2–49B.)

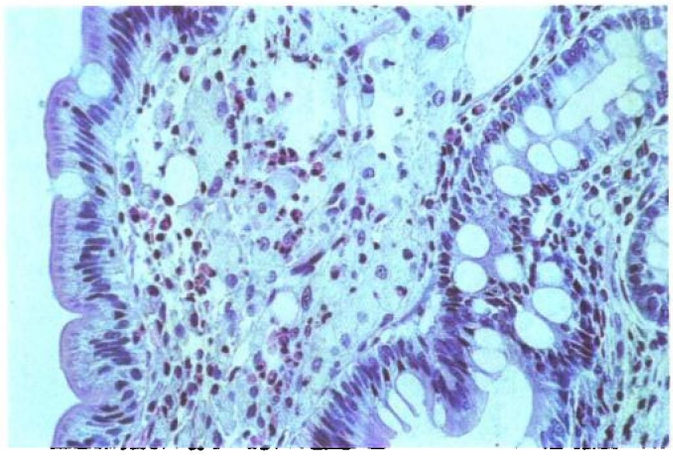

Color Plate 11. **Whipple's disease.** Histologic section of small intestine contains collection of foamy histiocytes and clear spaces in the lamina propria. (See page 159, Fig. 3–18.)

Color Plate 12. **Melanosis coli.** Gross photograph of colonic mucosa shows dark pigmentation. (See page 178, Fig. 3–30A.)

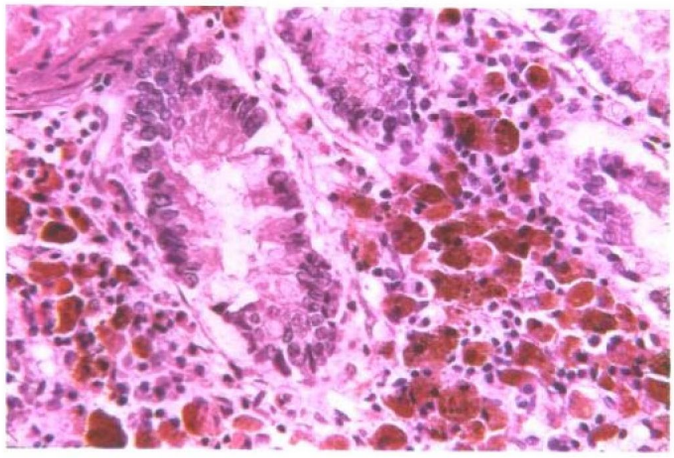

Color Plate 13. **Melanosis coli.** Histologic section shows colonic mucosa with numerous pigmented macrophages in the lamina propria. (See page 178, Fig. 3–30B.)

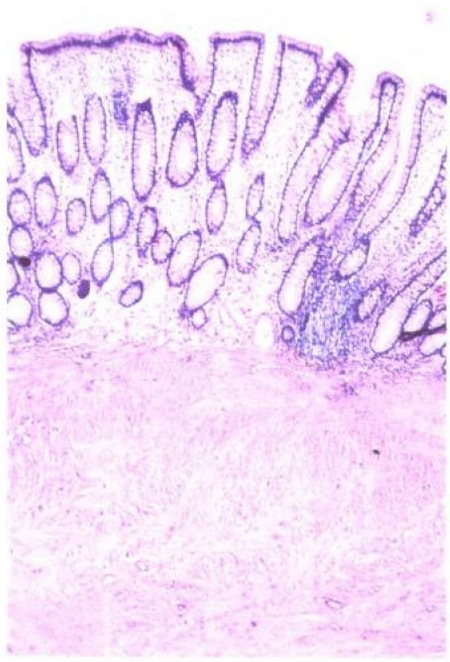

Color Plate 14. **Leiomyoma.** Low-power histologic section shows a well-defined submucosal spindle cell neoplasm. (See page 191, Fig. 34A.)

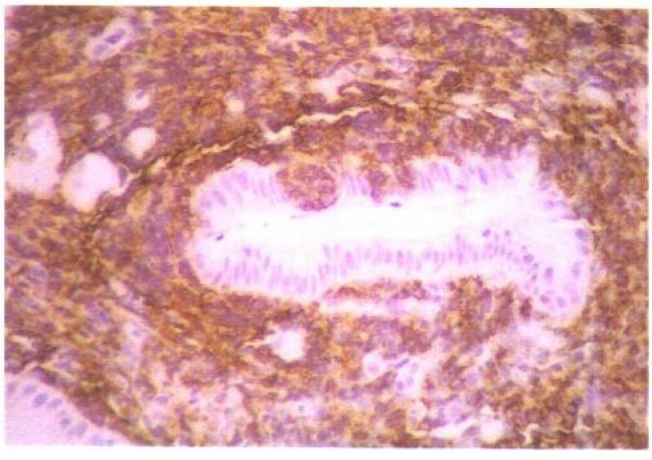

Color Plate 15. **Mucosa-associated lymphoid tissue (MALT) lymphoma.** Lymphoid infiltrate is diffusely positive for CD20 stain; the epithelial glandular cells are negative. (See page 193, Fig. 3–35B.)

Color Plate 16. **Mucosal-associated lymphoid tissue (MALT) lymphoma.** Cytokeratin stain highlights the epithelial glandular cells; the lymphoid component is negative. (See page 193, Fig. 3–35C.)

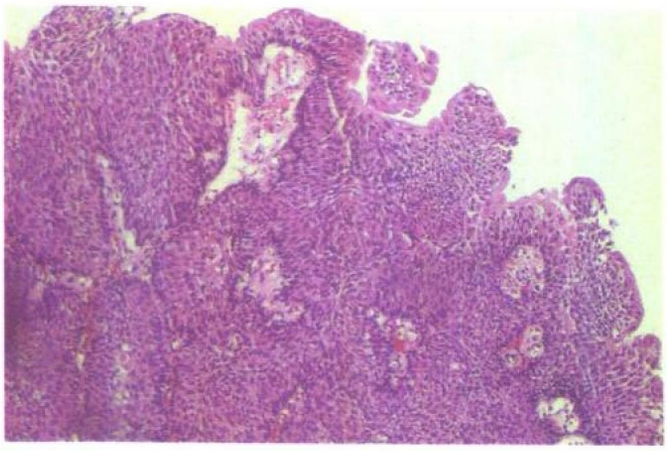

Color Plate 17. **Inverted papilloma.** Proliferation of urethelial cells originating from the surface epithelium with classical downgrowth pattern. (See page 215, Fig. 4–7.)

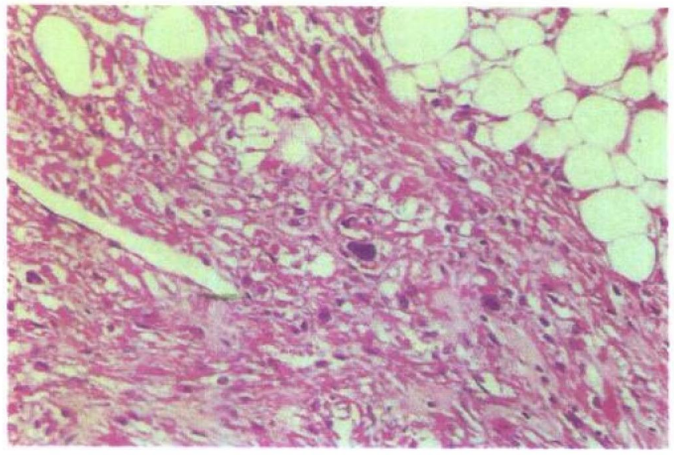

Color Plate 18. **Angiomyolipoma.** Classic angiomyolipoma of the kidney showing mature adipose tissue, smooth muscle, and blood vessels. (See page 229, Fig. 4–21.)

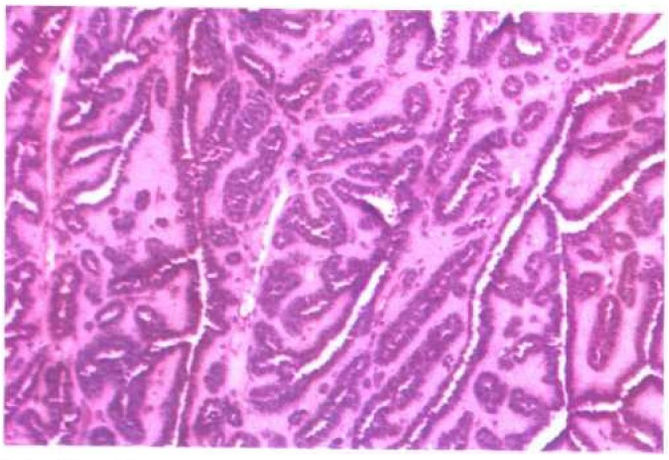

Color Plate 19. **Metanephric adenoma.** Proliferation of tubulopapillary structures within an acellular stroma background. (See page 231, Fig. 4–23.)

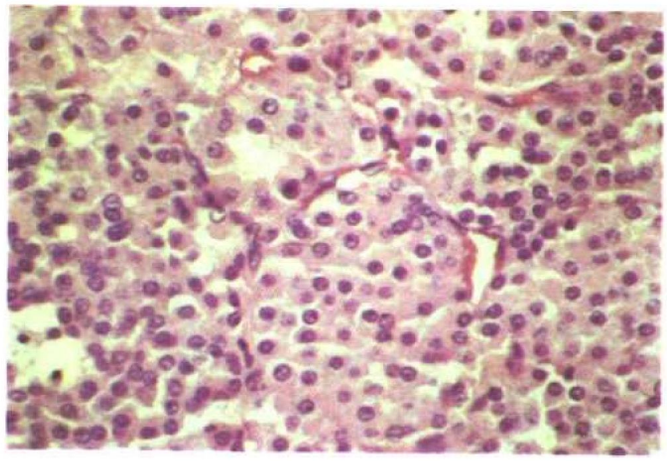

Color Plate 20. **Oncocytoma.** The tumor is composed of a monomorphic population of neoplastic cells with abundant eosinophilic granular cytoplasm. (See page 233, Fig. 4–24A.)

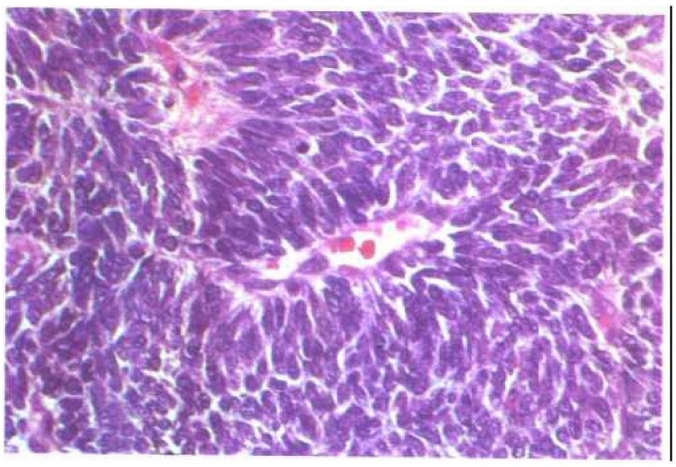

Color Plate 21. **Nephroblastoma (Wilms' tumor).** Wilms' tumor showing classical blastema component. Notice characteristic palisading of the nuclei around the blood vessels. (See page 239, Fig. 4–28B.)

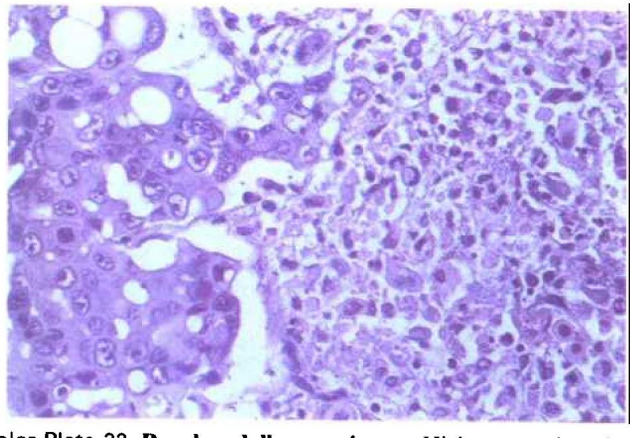

Color Plate 22. **Renal medullary carcinoma.** High-power view shows neoplastic cells with large amount of eosinophilic cytoplasm, pleomorphic nuclei with vesicular chromatin pattern, and prominent nucleoli resembling testicular yolk sac tumor. (See page 244, Fig. 4–32B.)

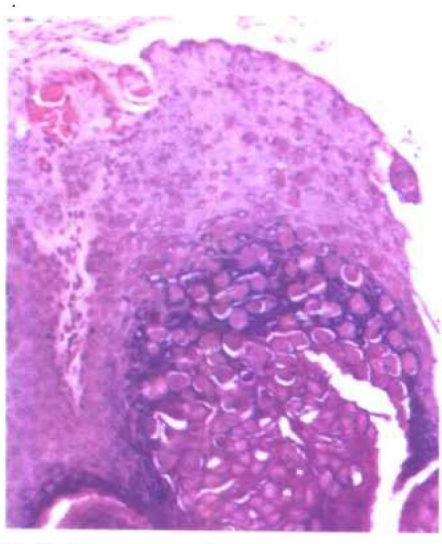

Color Plate 23. **Molluscum contagiosum.** Marked acanthosis with classic eosinophilic intracytoplasmic inclusions. (See page 260, Fig. 5–3.)

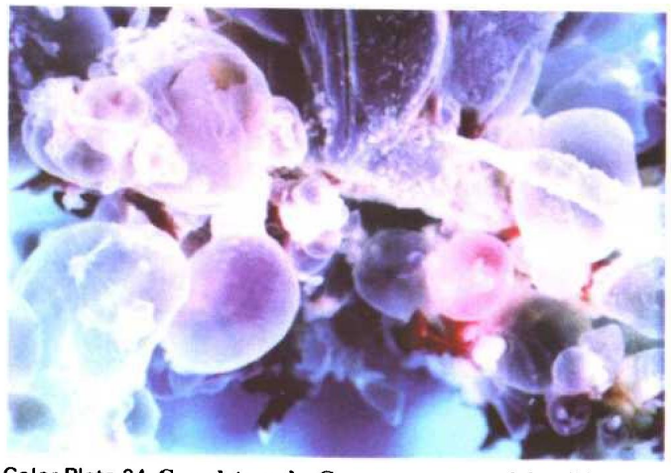

Color Plate 24. **Complete mole.** Gross appearance of the villi showing marked hydropic change reminiscent of bunches of grapes. (See page 309, Fig. 5–40A.)

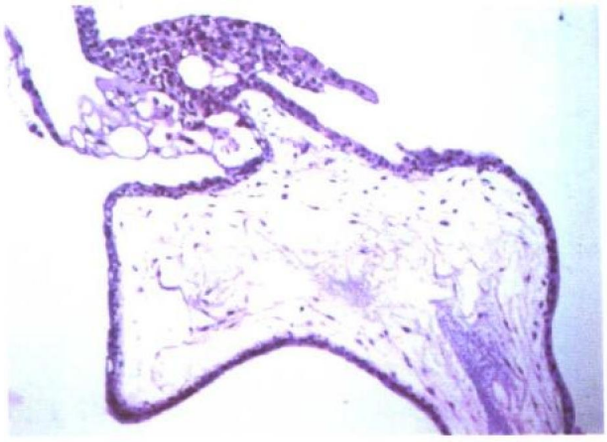

Color Plate 25. **Complete mole.** Villi show marked stromal edema. Trophoblast proliferation is noted. (See page 309, Fig. 5–40B.)

Color Plate 26. **Adult granulosa cell tumor.** (gross photograph) Cut surface shows a well-circumscribed yellow, lobulated, solid tumor mass. (See page 335, Fig. 5–56A.)

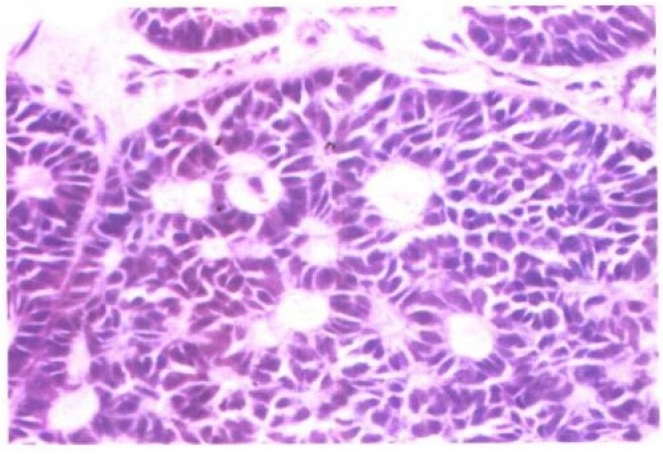

Color Plate 27. **Adult granulosa cell tumor, microfollicular variant (Call-Exner bodies).** (See page 335, Fig. 5–56B.)

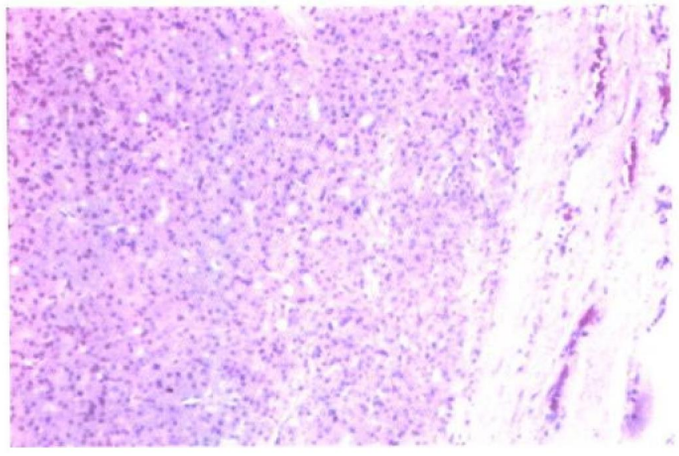

Color Plate 28. **Hürthle cell adenoma.** Low-power view shows a well-encapsulated tumor. (See page 383, Fig. 6–9A.)

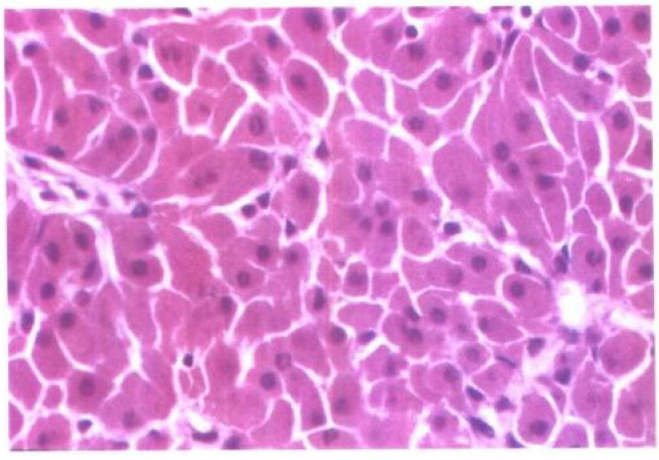

Color Plate 29. **Hürthle cell adenoma.** High-power view shows classic Hurthle cells with abundant eosinphilic granular cytoplasm. (See page 383, Fig. 6–9B.)

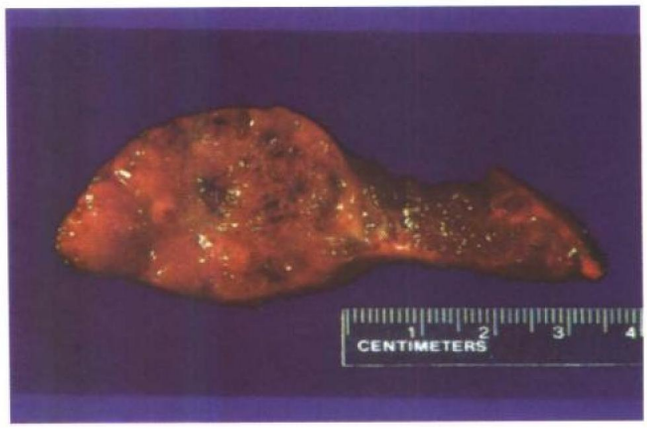

Color Plate 30. **Parathyroid adenoma.** Gross photograph shows a well-circumscribed mass. (See page 396, Fig. 6–19A.)

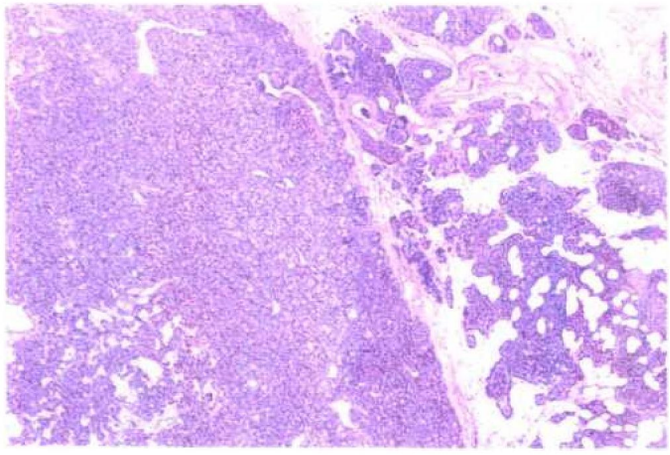

Color Plate 31. **Parathyroid adenoma.** Low-power view shows a well-defined mass surrounded by normal parathyroid tissue. (See page 396, Fig. 6–19B.)

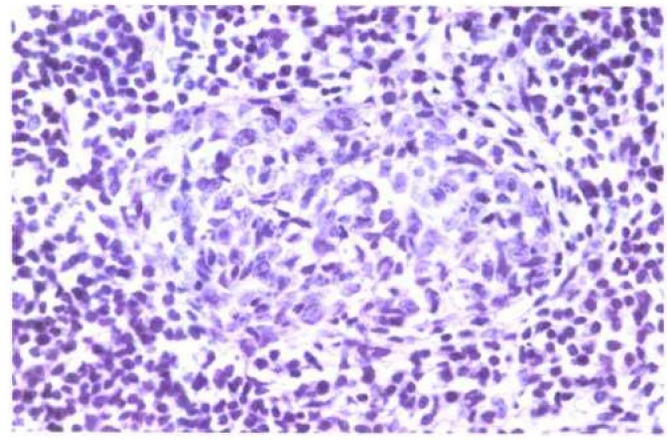

Color Plate 32. **Benign lymphoepithelial lesion.** High-power view shows epimyoepithelial island surrounded by small lymphoid cells. (See page 399, Fig. 6–22.)

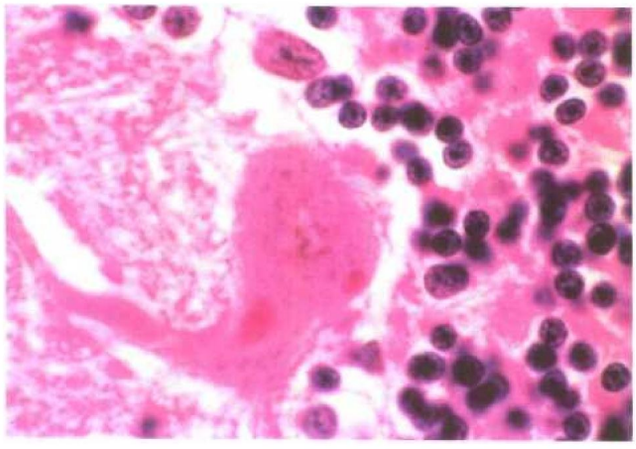

Color Plate 33. **Rabies encephalitis.** Classic intracytoplasmic inclusions in cytoplasm of the Purkinje cell of the cerebellum. (See page 508, Fig. 7–26D.)

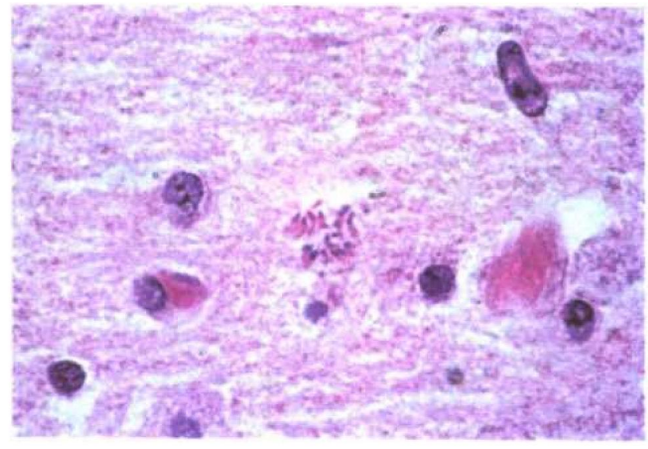

Color Plate 34. **Toxoplasmosis.** A cluster of *Toxoplasma* organisms is present lying free in the neuropil. (See page 508, Fig. 7–26E.)

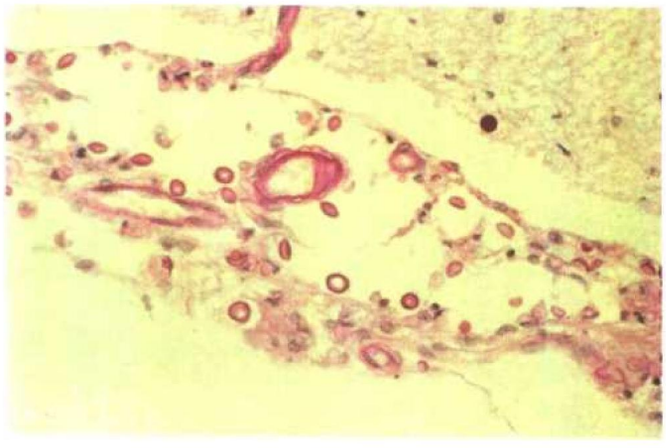

Color Plate 35. ***Cryptococcus* meningitis.** Mucin stain shows numerous round microorganisms. Notice the lack of staining of the capsule and the absent inflammatory response. (See page 509, Fig. 7–26H.)

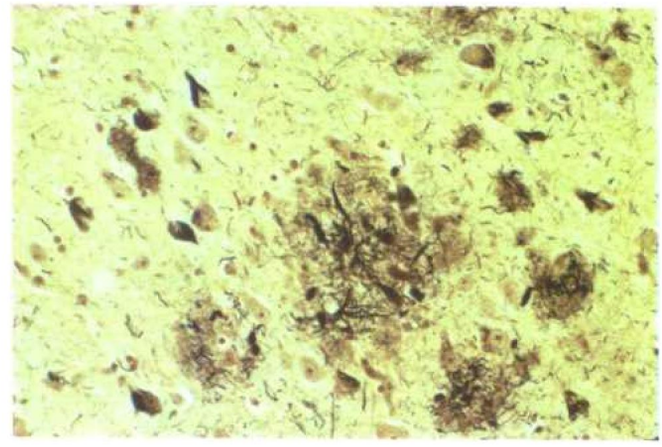

Color Plate 36. **Alzheimer's disease.** Scattered neuritic plaques and neurofibrillary tangles in the hippocampus. (Modified Bielschowsky stain) (See page 516, Fig. 7–31A.)

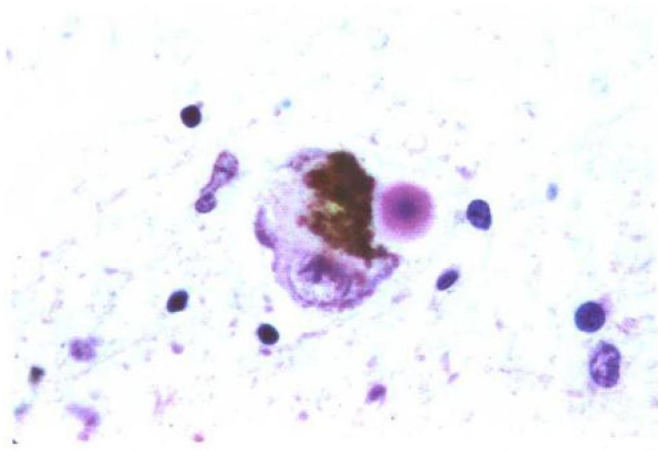

Color Plate 37. **Parkinson's disease.** A pigmented substantia nigra neuron containing a classic Lewy body in the cytoplasm. Note the brightly eosinophilic body surrounded by a halo. (See page 516, Fig. 7–31B.)

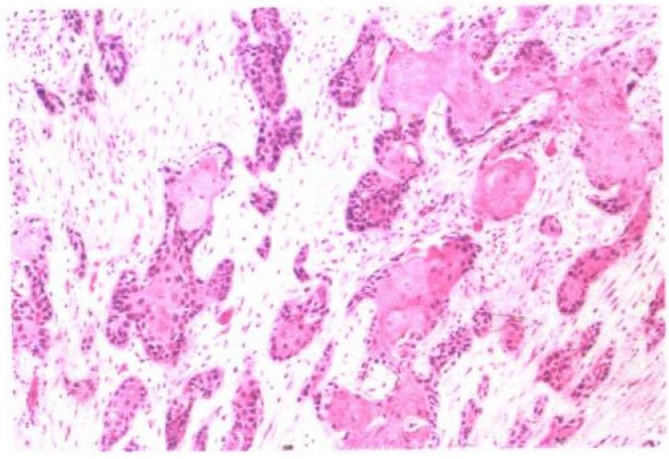

Color Plate 38. **Squamous cell carcinoma of the prostate.** Low-power view shows an infiltrative squamous cell carcinoma. Keratin formation is present in this case. (See page 548, Fig. 8–6.)

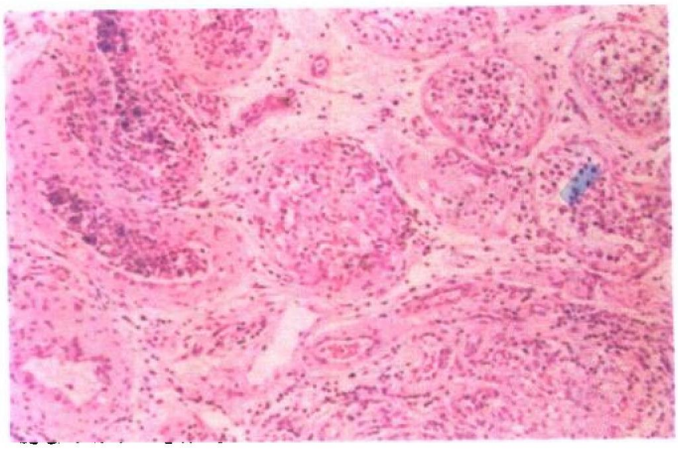

Color Plate 39. **Idiopathic granulomatous orchitis.** Low-power view shows interstitial fibrosis, focal tubular atrophy, and rare noncaseating granulomas. (See page 553, Fig. 8–11.)

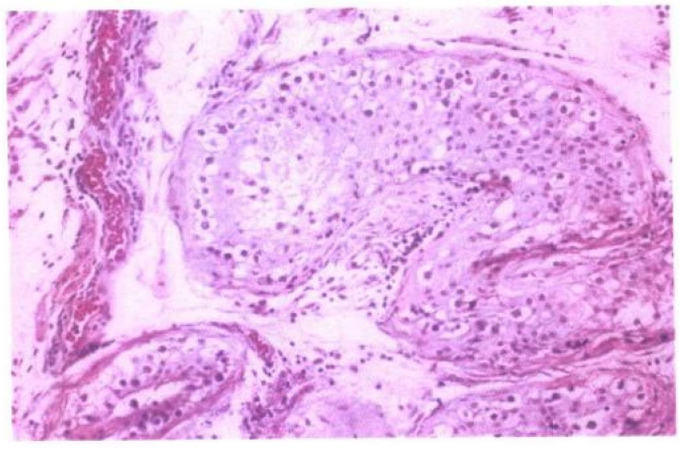

Color Plate 40. **Intratubular germ cell neoplasia (IGCNU).** Large malignant cells with vacuolated cytoplasm scattered along the basement membrane of the seminiferous tubules. (See page 556, Fig. 8–15.)

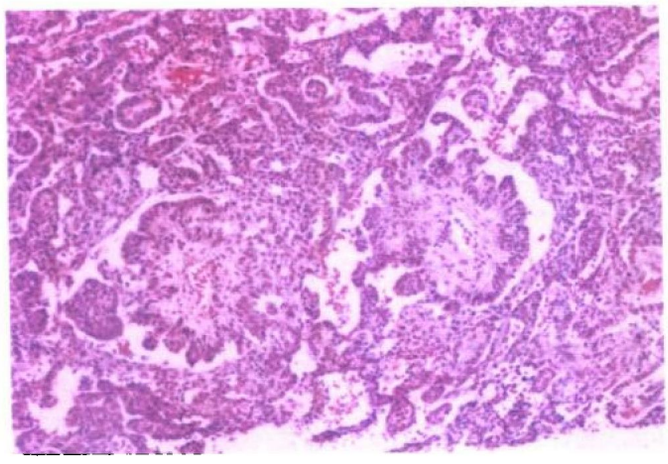

Color Plate 41. **Yolk sac tumor.** Cross section of a Schiller-Duval body. (See page 560, Fig. 8–18B.)

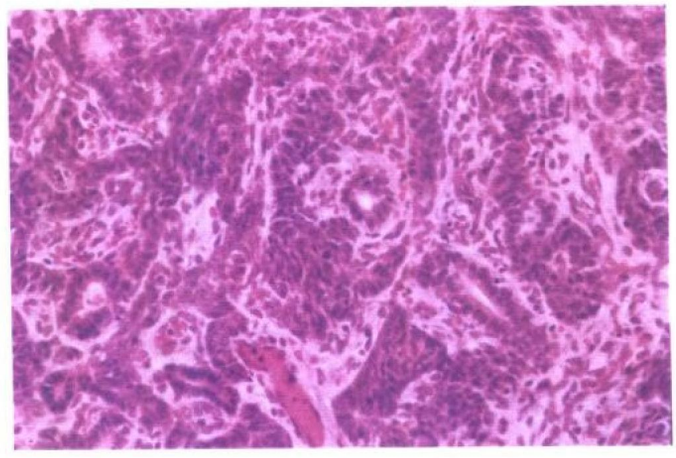

Color Plate 42. **Immature teratoma.** Low-power view shows immature fetal neuroepithelium and undifferentiated blastema tissue. (See page 561, Fig. 8–19B.)

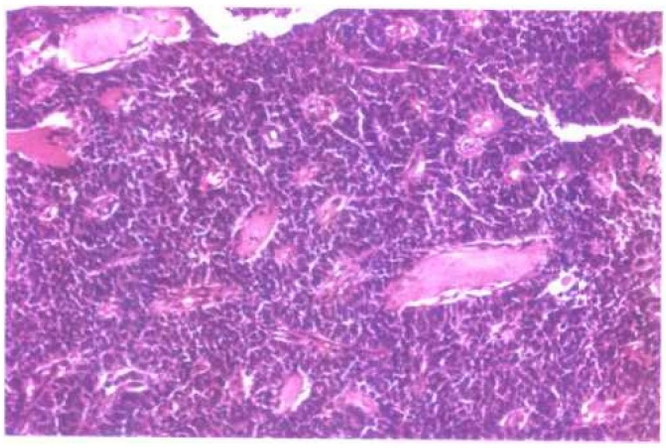

Color Plate 43. **Granulosa cell tumor, adult type.** Microfollicular pattern with Call-Exner bodies. (See page 566, Fig. 8–23.)

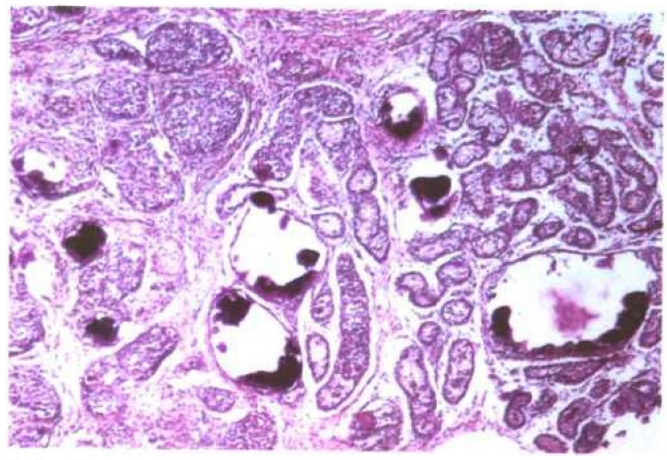

Color Plate 44. **Gonadoblastoma.** Low-power view shows Sertoli-like pattern and microcalcifications. (See page 567, Fig. 8–24A.)

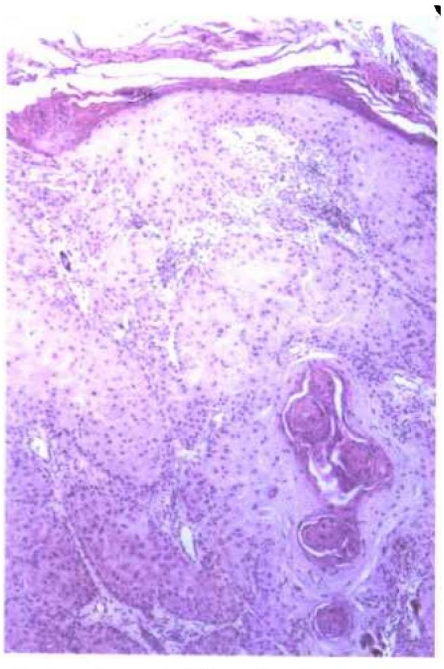

Color Plate 45. **Invasive well-differentiated squamous cell carcinoma.** (See page 585, Fig. 8–43A.)

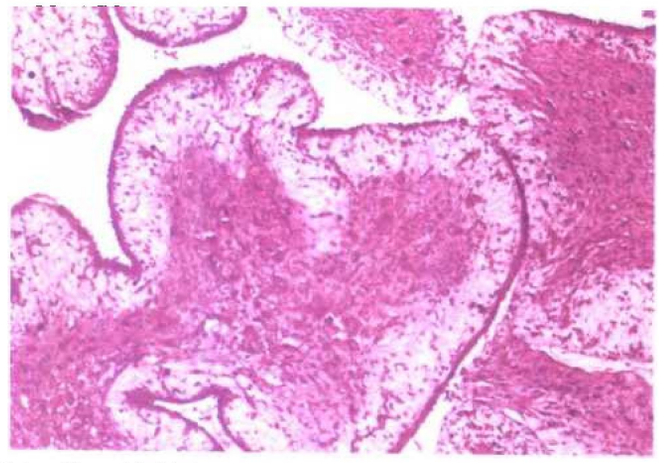

Color Plate 46. **Malignant phyllodes tumor.** The tumor displays leaf-like pattern with highly cellular stroma and cytologic pleomorphism. (See page 607, Fig. 9–16B.)

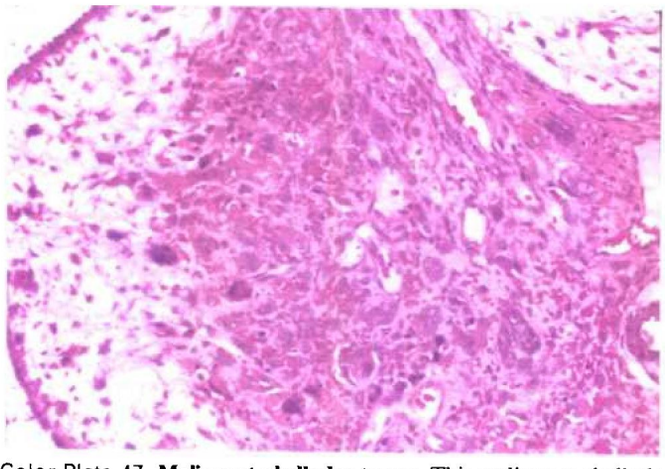

Color Plate 47. **Malignant phyllodes tumor.** This malignant phyllodes tumor shows marked nuclear pleomorphism and mitotic activity of the stromal component. (See page 607, Fig. 9–16C.)

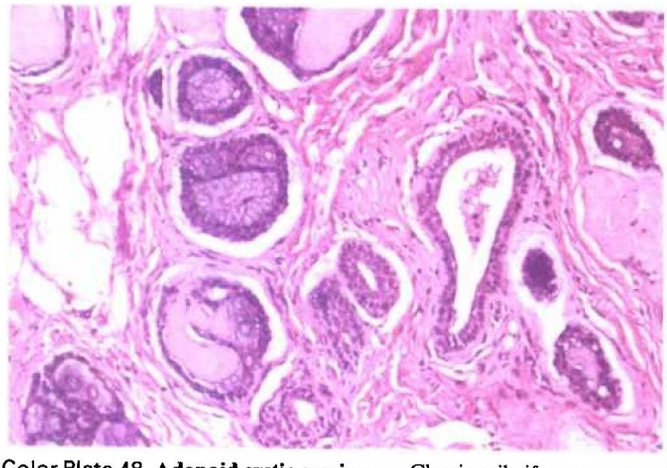

Color Plate 48. **Adenoid cystic carcinoma.** Classic cribriform pattern of adenoid cystic carcinoma. Notice the eosinophilic basement membrane-like material. (See page 622, Fig. 9–28.)

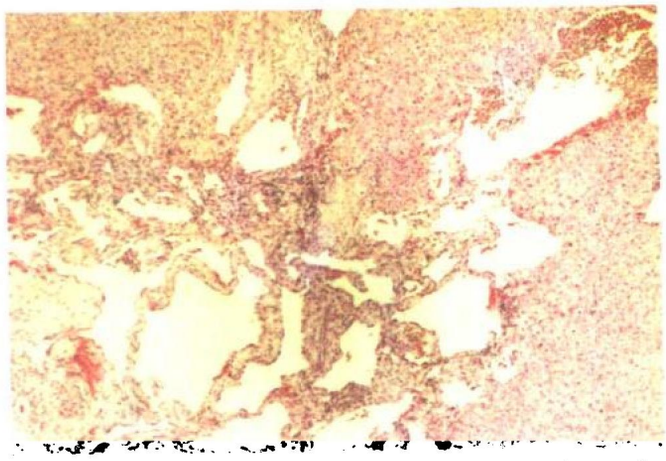

Color Plate 49. **Liver hemangioma.** Lower-power photomicrograph of a liver section shows classic hemangioma composed of dilated vascular spaces. (See page 643, Fig. 10–7.)

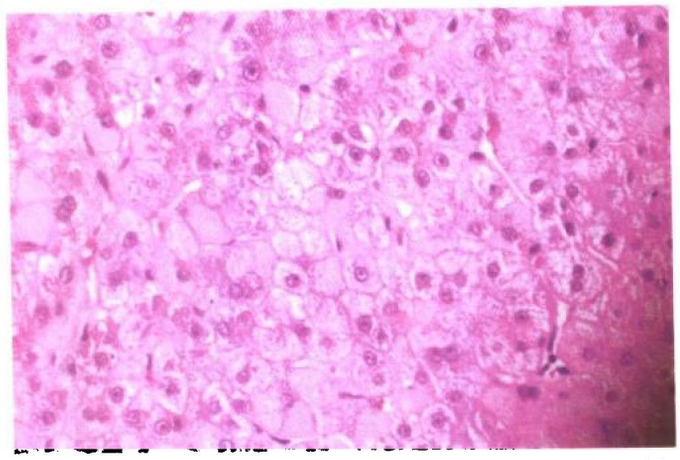

Color Plate 50. **Acute hepatitis.** Classic ballooning degeneration of the hepatocytes. (See page 653, Fig. 10–16A.)

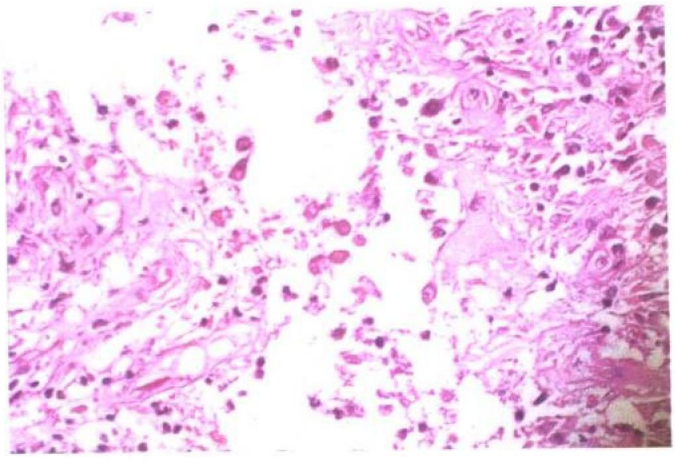

Color Plate 51. **Amoebic abscess.** Liver tissue showing necrotic debris with trophozoites at the center of the microphotograph. (See page 654, Fig. 10–18B.)

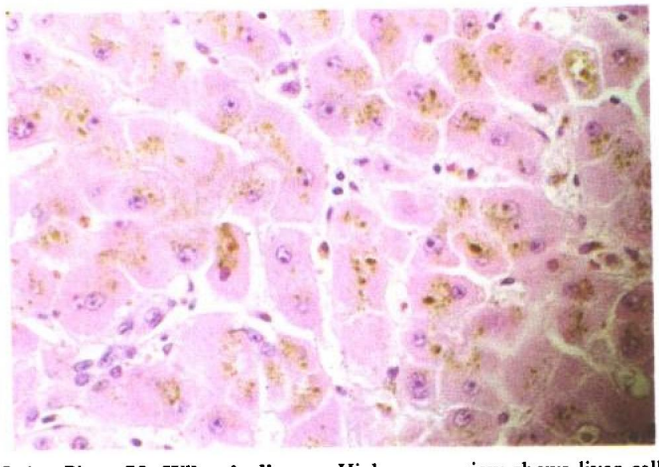

Color Plate 52. **Wilson's disease.** High-power view shows liver cells containing cytoplasmic copper pigment. (See page 659, Fig. 10–22.)

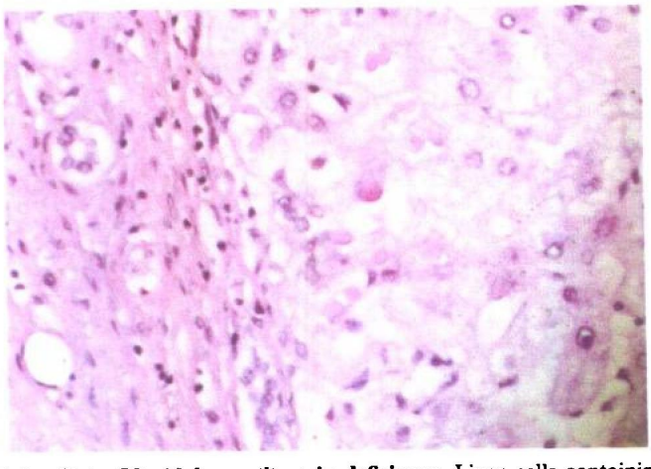

Color Plate 53. **Alpha$_1$-antitrypsin deficiency.** Liver cells containing intracytoplasmic eosinophilic inclusions in the periportal area. (See page 660, Fig. 10–23.)

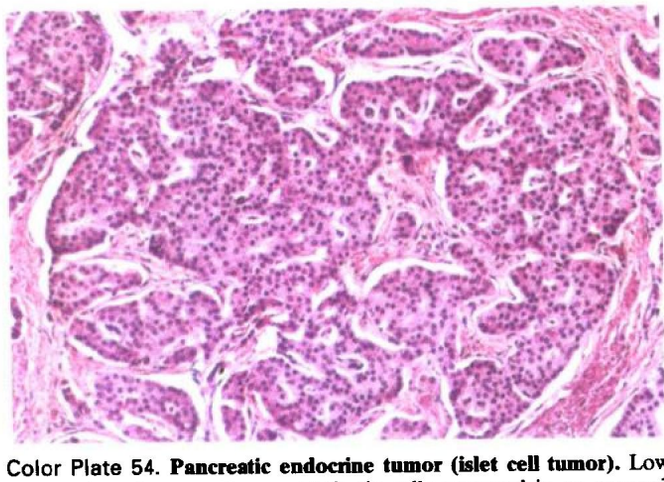

Color Plate 54. **Pancreatic endocrine tumor (islet cell tumor).** Low-power view shows uniform, neoplastic cells arranged in an organoid pattern. (See page 680, Fig. 11–15.)

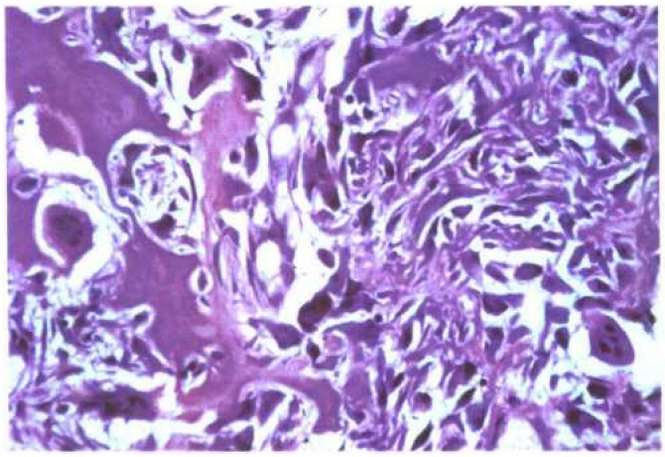

Color Plate 55. **Osteoid osteoma.** Section shows a central nidus of thin bony trabeculae with prominent benign osteoblastic rimming. (See page 690, Fig. 12–2.)

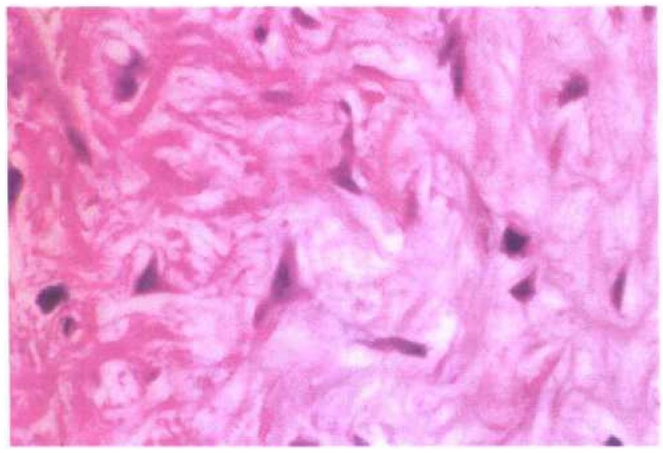

Color Plate 56. **Chondromyxoid fibroma.** Section from another example of chondromyxoid fibroma shows the stellate cells in the stroma. (See page 705, Fig. 12–11B.)

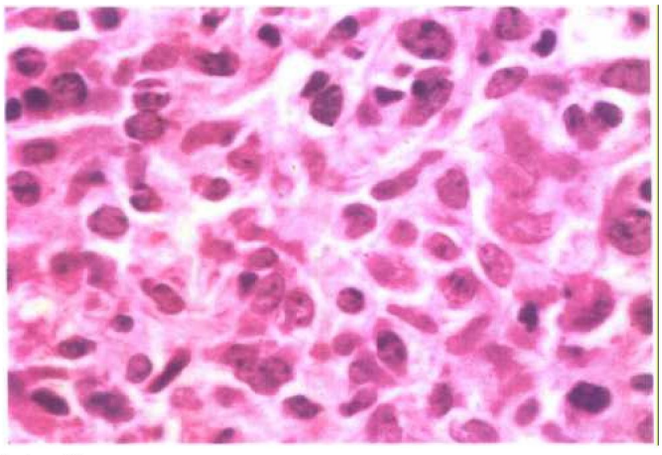

Color Plate 57. **Lymphoma, large cell type.** High-power view shows sheets of large atypical lymphoid cells. (See page 727, Fig. 12–30.)

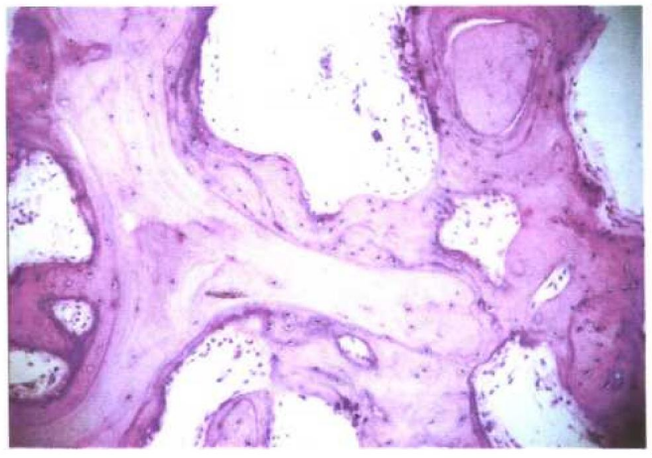

Color Plate 58. **Paget's disease of bone.** Section shows irregularly thickened bony trabeculae with prominent cement lines. (See page 732, Fig. 12–34.)

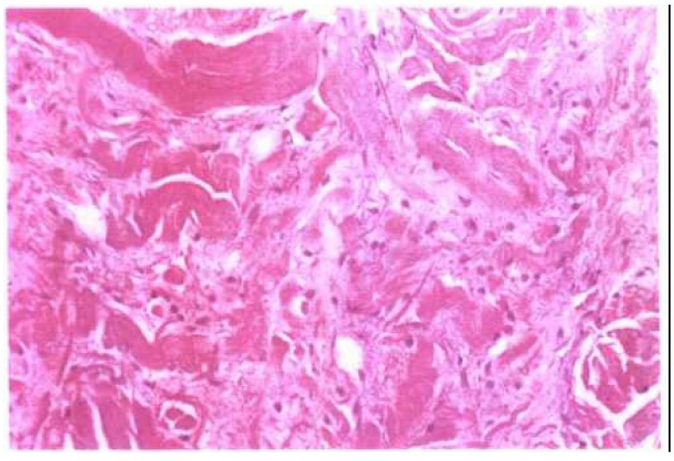

Color Plate 59. **Elastofibroma.** High-power view shows abnormally thickened and fragmented elastic fibers in a collagenous background. (See page 753, Fig. 13–4A.)

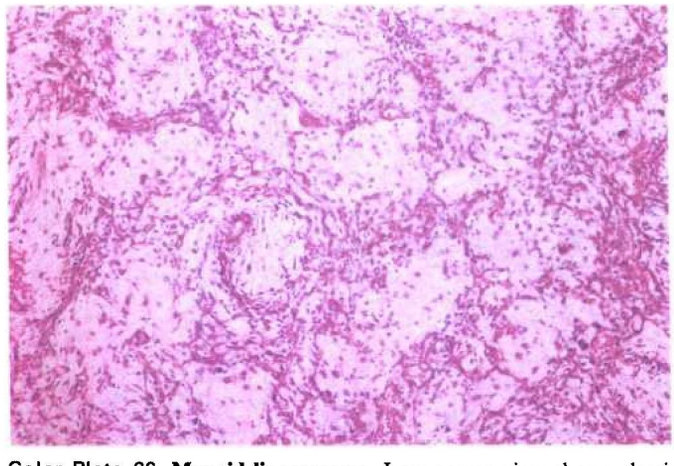

Color Plate 60. **Myxoid liposarcoma.** Low-power view shows classic myxoid background and vascular pattern. (See page 768, Fig. 13–15B.)

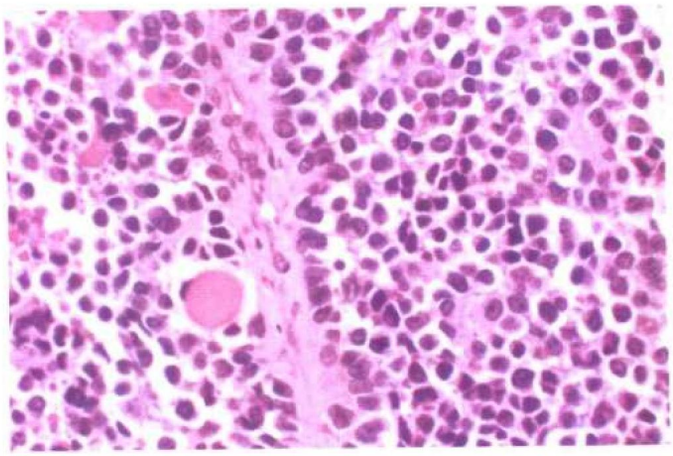

Color Plate 61. **Rhabdomyosarcoma.** Histologic section shows small round blue cell proliferation and scattered cells with abundant granular cytoplasm, characteristic of skeletal muscle differentiation. (See page 774, Fig. 13–20A.)

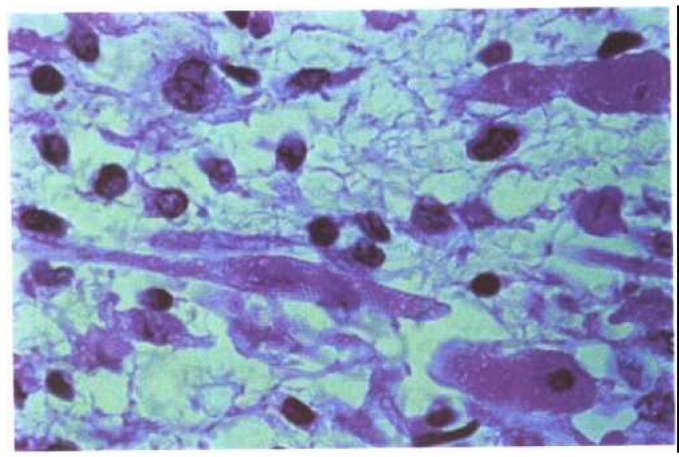

Color Plate 62. **Rhabdomyosarcoma.** High-power view of spindle-shaped cells with abundant granular cytoplasm, "strap cell." (See page 774, Fig. 13–20B.)

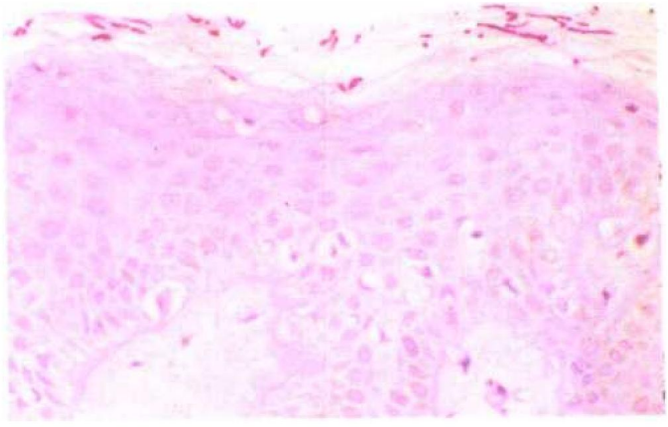

Color Plate 63. **Dermatophytosis.** PAS stain shows the presence of fungal hyphae and spores within the cornified layer. (See page 805, Fig. 14–1B.)

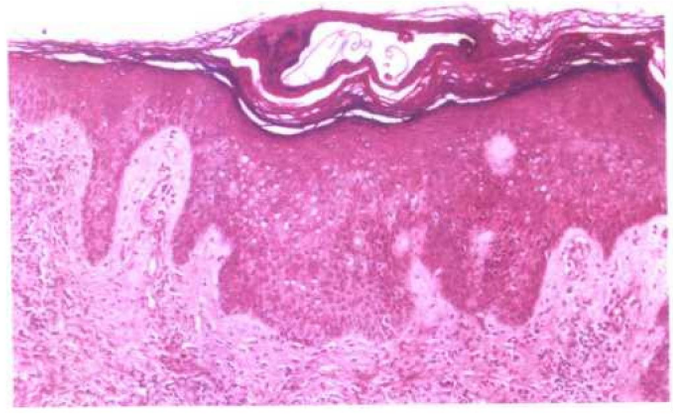

Color Plate 64. **Scabies.** Section shows a parakeratotic burrow containing body parts of the mite of scabies. A moderately dense dermal infiltrate containing eosinophils is characteristic. (See page 825, Fig. 14–22.)

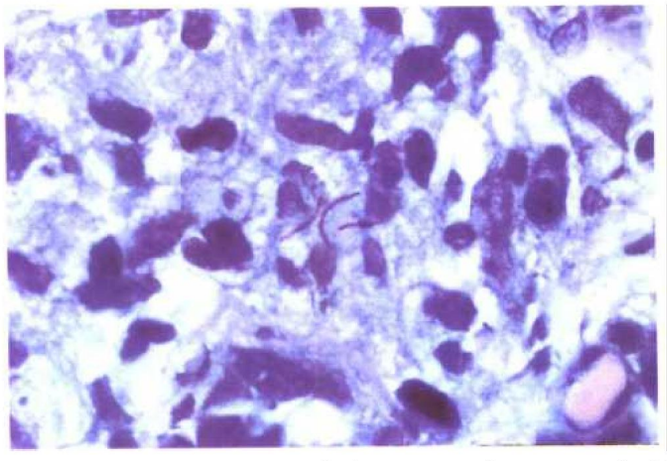

Color Plate 65. **Leprosy.** AFB stain demonstrates the presence of acid-fast bacilli within the cytoplasm of some of the histiocytes. (See page 831, Fig. 14–31B.)

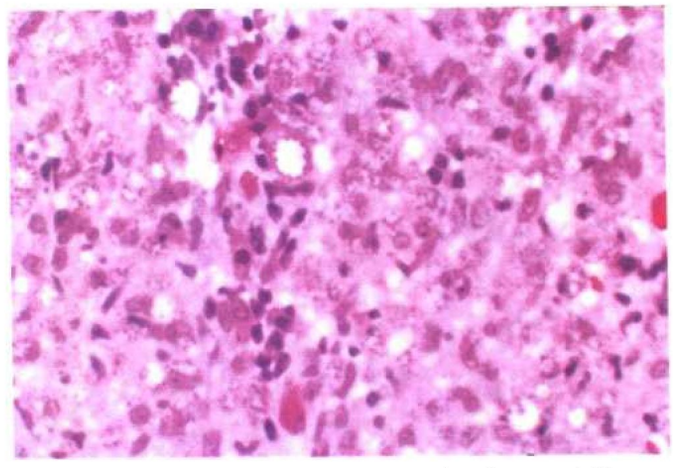

Color Plate 66. **Leishmaniasis.** High-power view shows an infiltrate of plasma cells and histiocytes. Within the cytoplasm of the histiocytes there are organisms that are 2 to 4 microns in size. A Giemsa stain can also be used to highlight the parasite. (See page 834, Fig. 14–33.)